Matrix Photochemistry of Cycloheptatriene: Site Effects

ARTICLE *in* THE JOURNAL OF PHYSICAL CHEMISTRY A · MAY 1998

Impact Factor: 2.69 · DOI: 10.1021/jp981100i

3 AUTHORS, INCLUDING:

Uri Samuni
City University of New York - Queens College
43 PUBLICATIONS **1,503** CITATIONS
SEE PROFILE

Yehuda Haas
Hebrew University of Jerusalem
66 PUBLICATIONS **1,206** CITATIONS
SEE PROFILE

Matrix Photochemistry of Cycloheptatriene: Site Effects

Uri Samuni, Smadar Kahana, and Yehuda Haas*

Department of Physical Chemistry and the Farkas Center for Light Induced Processes, The Hebrew University of Jerusalem, Jerusalem, Israel 91904

Received: February 11, 1998; In Final Form: March 31, 1998

An experimental study of CHT photolysis at 2537 Å in argon and nitrogen (N_2) matrices is presented. The sole IR detectable product is identified as BCHD: bicyclo[3.2.0]hepta-2,6-diene. It is found that CHT molecules trapped in spectroscopically distinct sites were converted to the product at different rates. In the initial stages of the photolysis, the population of some CHT trapping sites increased, indicating site population transfer. In the long run, however, all sites were depleted. Molecular dynamics simulations are performed to estimate the structure of the different sites, and together with a kinetic model, are used to account for the UV induced changes. A tentative energy level diagram of the system is offered, in an attempt to rationalize the total absence of toluene which is formed predominantly in the gas-phase irradiation of CHT at this wavelength. The "twin state" concept is instrumental in this rationalization.

1. Introduction

The photochemistry of cycloheptatriene has been studied extensively in the gas and solution phases.[1−8] The molecule is a seven membered ring conjugated hydrocarbon, and as such can undergo a variety of photochemical transformations, summarized in Figure 1. In the ground state it has a boat form with C_s symmetry,[9,10] and can undergo facile conformational isomerization. The barrier for this isomerization has been estimated from NMR studies to be about 6 kcal/mol,[11,12] a value supported by ab initio calculations.[13,14] The near UV spectrum ($\epsilon_{280} = 3470$ l mol^{-1} cm^{-1}) is structureless in the gas phase, indicating rapid photochemical activity, a conclusion supported by the low fluorescence quantum yield (1.4×10^{-6},[15]). INDO/S calculations show that this UV band is actually due to two nearby transitions, both of $\pi-\pi$ character due to the conjugated system.[16] At the Franck−Condon region, the lower has A″ and the higher A′ symmetry. The stronger transition observed at about 6 eV is of ethylenic nature.

In liquid solutions, photoexcitation leads to an efficient suprafacial (1,7) migration of the hydrogen atom[4] (Figure 1) as well as to a less efficient ring closure leading to the bicyclo-[3.2.0]hepta-2,6-diene (BCHD)[2]. The sigmatropic 1,7 hydrogen shift is reported to be ∼500 times faster than ring closure.[4] Resonance Raman experiments[15,17] indicate that immediately after excitation the molecule flattens, as evidenced by strong scattering due to ring planarization modes. This step is believed to be extremely rapid (∼20 fs), involving a second excited state, probably the A′ state that is lower in energy than the A″ state at the planar geometry, as indicated by preliminary ab initio calculations. The hydrogen migration step follows, leading to a vibrationally excited ground-state product that is relaxed with a time constant of 26 ps.[8]

Extended irradiation of CHT in liquid solutions leads to the formation of BCHD as the major final product,[1] others being toluene and a polymer. Under certain conditions the conversion efficiencies of 30% and chemical yields of about 90%[7] were achieved, though a quantitative quantum yield was not reported. It is expected to be very small (∼0.002), based on the fact that BCHD formation is slower by a factor of ∼500 than hydrogen migration.[4] BCHD was identified based on its physical properties, UV, IR, and NMR spectra.[18] Photosensitization by benzophenone or triphenylene did not lead to any product, showing that the triplet state is not involved in this reaction. Efforts to identify any reactive intermediates failed, even at low-temperature experiments.[7] The thermal formation of BCHD from CHT was not reported. Heating BCHD yields CHT, with an activation energy of 39.5 kcal/mol,[19] demonstrating the thermal stability of this rather strained molecule.

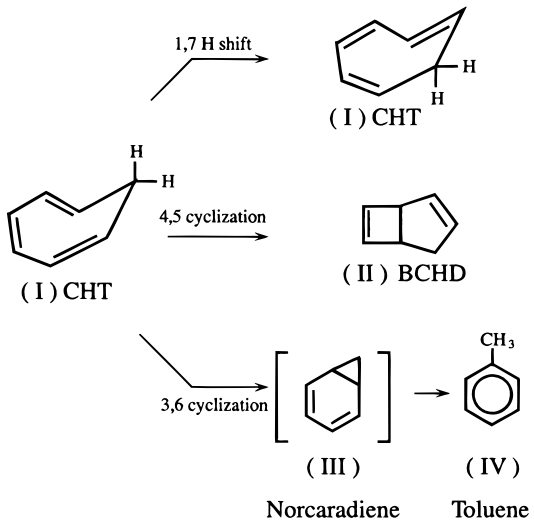

Figure 1. Three major reaction channels observed in the UV photochemistry of CHT: Top, 1,7 hydrogen shift; middle, 4,5 cyclization (formation of a molecule in which a four membered ring shares two carbon atoms with a five membered ring); bottom, 3,6 cyclization forming norcaradiene, which relaxes to toluene.

The gas-phase photochemistry of CHT was first studied by Srinivasan,[2] who found that BCHD and toluene were the major products, the latter being the dominant product. BCHD yield increased with pressure but never exceeded 5% of the products. He suggested that toluene was formed from vibrationally excited ground state CHT molecules, following rapid internal conversion. This conclusion was amply supported by subsequent time-

S1089-5639(98)01100-1 CCC: $15.00
Published on Web 05/28/1998

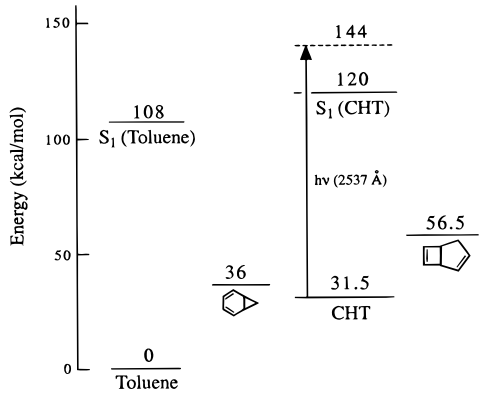

Figure 2. Energetics of some C_7H_8 molecules relevant to cycloheptatriene photochemistry (see text for literature sources, which are partly experimental and partly calculated).

resolved[20] and steady-state[21] experiments on CHT and some of its derivatives. The conversion to toluene tends to unit quantum yield at low pressures and is quenched by added gases.[3] At very high pressures the conversion to toluene decreases and appears to approach a limiting value of 3%,[5] close to the liquid-phase value reported by Srinivasan. The isomerization of CHT to toluene is exothermic (31.5 kcal/mol) with an estimated activation energy in the ground state of 50 kcal/mol,[3] in agreement with thermal studies.[22] The thermal isomerization may involve a norcaradiene intermediate which opens to the much more stable toluene (Figure 1). The energy difference between CHT and norcaradiene in the ground state is estimated to be small, about 4.5 kcal/mol.[23]

Figure 2 shows an energy diagram relevant for CHT photochemistry. The enthalpies of formation of the different species are shown relative to the thermodynamically most stable isomer, toluene.

The rich photochemistry of CHT makes it an interesting candidate for the study of matrix and site effects on the course of a chemical reaction.[24] Environmental effects which are inherent in condensed phase may well determine the outcome of a chemical reaction, favoring a specific channel over another. In a matrix, the cage effect is dominant, favoring isomerization over dissociation in many cases.[25−28] Vibrational relaxation is usually quite efficient, tending to reduce the yield of reactions from vibrationally excited molecules. Thus, the matrix may simplify a complicated reaction scheme by channeling it to one favorite route.

Matrix isolation is also amenable to molecular dynamics simulations, which help in analyzing possible site effects, as demonstrated recently.[29−31] Much insight was gained, particularly in identifying and characterizing different trapping sites and relating them to reaction feasibility and even different reaction rates. Some recent experimental studies have emphasized the importance of site effects in understanding thermal[32] and photochemical[33] effects on the reactivity of matrix trapped molecules. Site effects reported in this work are also qualitatively supported by MD simulations.

The strong medium effect on the product distribution of CHT photochemistry, makes it a suitable candidate for testing matrix effects. In this paper we show that deposition of CHT in an argon or N_2 matrix leads to the formation of several trapping sites. Long term UV irradiation results in almost quantitative transformation to BCHD, but the short term photochemical activity of CHT in different sites varies strongly. In fact, it is found that the population of some of the trapping sites initially increases upon irradiation, while others are depleted. This trend is qualitatively accounted for by MD simulations of the trapping site structure in an argon matrix.

2. Experimental and Computational Details

CHT vapor was premixed with the carrier gas in a separate container at the desired concentration, and the mixture was deposited onto a KBr window held at a predetermined temperature (typically 23 or 14 K) by a helium closed cycle cryostat (Air Products CS202). The temperature was controlled by a Lake Shore Cryogenics Temperature Controller (Model 330) autotuning to within ±0.5 K. The deposition rate was controlled by a variable leak valve (VAT, series 69) in the range of 2−10 mmol/h, with the deposition time varying between 2 and 4 h. Three characteristic temperatures were used in the experiments: T_d, the deposition temperature; T_s, the temperature at which the spectra were recorded, and T_{ir}, the temperature of the matrix during irradiation period. The infrared spectrum of the resulting matrix was recorded by a Fourier transform spectrometer (Nicolet Model 520, 0.5 cm^{-1} resolution) in the spectral range 400−4000 cm^{-1}. Irradiation source was a low pressure mercury arc (essentially pure 2537 Å, a filter was used to suppress the 1849 Å component) and irradiation time varied between 1 and 150 h, during which spectra were taken periodically to monitor the progress of the photochemical reaction. CHT (Fluka 95%), Argon (Matheson 99.9995%), and Nitrogen (Gordon-Gas, either 95.5 or 99.999%) were used as received.

Molecular dynamics simulations were performed as previously described.[34−36] Specific details are provided in section 5.

Ab initio calculations were carried out using the Gaussian 94 program package,[37] at the HF or HF-MP2 levels and by the density functional theory at the B3LYP level. Several basis sets were used, the largest of which was 6-311G*.[38] Complete structural optimization was performed for each species and vibrational frequencies were calculated from the Hessian matrix using the harmonic approximation at the optimized geometry. No imaginary frequencies were found in the calculation, showing that the optimized structure was indeed a minimum. The resulting frequencies were uniformly scaled by 0.988 for the B3LYP/6-311G* calculation.

3. Results

3.1. CHT in an Argon Matrix. *3.1.1. The IR Spectrum of CHT in an Argon Matrix.* The IR spectrum of CHT is well-known in the gas and liquid phase. A portion of the argon trapped spectrum of this molecule is compared with a quantum chemical calculated one in Figure 3: most bands are rather weak, only two or three are relatively strong. Table 1 lists the experimental transitions, alongside with solution phase literature data and a quantum chemical calculation. The most intense bands, centered around 710 and 741 cm^{-1}, were chosen for a more detailed study. The quantum chemical calculation shows that the 710 cm^{-1} is due mostly to a combination of CH out-of-plane wag (umbrella mode) and in-plane symmetric stretch of the two carbon atoms adjacent to the CH_2 group. The other strong IR band, centered around 741 cm^{-1}, is also due mainly to CH out-of-plane wag. Both bands were found to be split in the matrix into several subbands whose relative intensities were found to depend on the deposition conditions, mostly CHT concentration and deposition temperature. Figure 4 shows a higher resolution recording of these two IR bands obtained under different experimental conditions. The splittings observed are of the order of 1 cm^{-1}, very close to the 0.5 cm^{-1} spectral resolution of our spectrometer. It is likely that, under higher

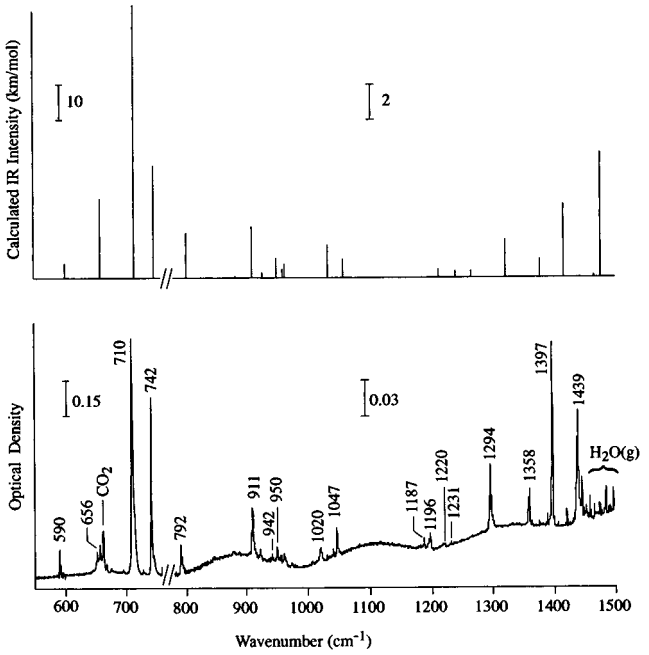

Figure 3. A portion of the IR spectrum of CHT in an argon matrix compared to a quantum chemical density functional theory calculation (B3LYP/6-311G* with a 0.988 correction applied).

resolution, more splittings may be observed. However, in this work we are interested in the gross photochemical consequences of site selection, rather than in full spectroscopic analysis.

The relative intensity of the three peaks is different when deposition is carried out at 14 K as can be seen from Figure 4b. Annealing of the matrix (to 38 K for 20 min) changes the relative intensity of the peaks: two decrease in intensity while the third (at 709.6 cm^{-1}) increases, dominating the spectrum (Figure 4c). This peak is the most intense when deposition is carries out at 23 K. It is noted that annealing also leads to the appearance of some blue shifted, broader weak peaks that are assigned to aggregates (dimers, trimers, etc.) of CHT. These peaks are found to further increase upon warming the matrix to 40 K.

3.1.2. Effects of Irradiation on the IR CHT Bands. UV light (2537 Å) irradiation of CHT in an argon matrix leads to an overall decrease in the area of the CHT bands and appearance of new product bands. In the initial phase of the irradiation, the relative intensity of the three CHT subbands of the 710 cm^{-1} feature changes considerably. Figure 5 shows the IR spectra of CHT in an argon matrix (deposited at 23 K, cooled to 13 K, and then irradiated at 13 K) in the 700−760 cm^{-1} region. After about 1 h of irradiation, the relative intensity of the CHT peaks changes (Figure 5b). The intensity of the 709.6 cm^{-1} peak (the dominant one under the deposition conditions) decreases absolutely and also relative to the other peaks. In contrast, the intensity of the 712.0 cm^{-1} peak increases both relatively and absolutely. It is interesting to note that irradiation appears to operate contrary to annealing: this subband is the same one that was observed to decrease upon annealing, while the 709.6 one increased. A similar effect can be seen for the 741 cm^{-1} band. The 741.6 peak (the dominant one under these conditions) decreases while the intensity of 742.9 cm^{-1} subband increases not only relatively, but also in absolute terms. Figure 5c shows the IR spectra of the same matrix after a prolonged irradiation (90 h). The CHT absorption bands are almost totally absent showing that the *absolute* increase of some of the CHT bands was only temporary and that a long enough irradiation leads to photochemical conversion of about 90% of the CHT molecules trapped in argon, regardless of trapping site. Similar data were also obtained upon irradiating the matrix at a higher temperature (23 K).

TABLE 1: Experimental and Calculated Vibrational Frequencies of CHT

experimental				calculated	
frequency[a] (cm^{-1})	approximate intensity	frequency[b] (cm^{-1})	normalized intensity	frequency[c] (cm^{-1})	intensity (km/mol)
				211	0.29
				292	0.69
				353	2.1
406	w, br[d]			413	0.58
420	s, br	423	5.3	427	6.8
589	ms	590	4.6	601	4.4
657	vs	656	16.4	660	22
710	vvs	710	100	715	75
743	vs	742	34	748	31
793	s	792	2.2	801	2.6
871	w	882	0.10		
905	s	911	3.6	910	3.0
				927	0.30
946	ms	942	0.2	950	1.1
		950	0.4	959	0.48
970	m			964	0.81
				980	0.01
1016	ms	1020	1.4	1032	1.9
1047	ms	1047	1.3	1057	1.1
		1187	0.4	1205	0.01
1191	ms	1196	0.9	1213	0.44
1216	m	1220	0.6	1240	0.38
1246	sh	1231	0.1	1264	0.39
1293	s	1294	4.1	1320	2.2
1352	ms	1358	2.0	1377	1.0
1392	s	1397	7.6	1415	4.2
				1466	0.13
1434	vs	1438	10.7	1477	7.2
1534	m			1557	0.29
1606	ms			1648	0.60
1688	ms			1657	0.64
		2830	1.4	2961	37
2841	s	2840	4.5		
		2850	6.7		
2884	s	2885	5.2	3052	25
		2896	7.7		
2969	s	2970	21		
				3085	0.74
2995	sh	3000	1.4	3091	4.0
3015	vs	3026	18	3098	12
3027	vvs	3036	30	3113	74
		3043	21	3120	57
3060	w	3067	2.6	3125	7.8

[a] Reference 45. [b] From CHT IR spectra in an argon matrix, this work. [c] B3LYP/6-311G* calculation, this work. [d] w = weak, br = broad, s = strong, ms = medium strong, vs = very strong, vvs = very very strong.

As the irradiation proceeds, product bands are observed to appear and grow. One of the more intense product bands, at about 728 cm^{-1} is shown in Figure 5c; it is also split into several subbands.

Figure 6 shows the normalized total band area of the reactant, CHT (the 710 cm^{-1} band) and of the product (the 782 cm^{-1} band) as a function of irradiation time. It was found that the decay of CHT and the rise of the product follow first-order kinetics, with the *same* rate constant $(8.5 \pm 0.3) \times 10^{-3}$ h^{-1}) within experimental error. The numerical values of these rate constants were dependent on the experimental conditions (light intensity, concentration, temperature), but the equality of the decay and formation rate constants appears to be universal. However, closer inspection revealed that *individual subbands exhibited different kinetic characteristics*. Figure 7 shows that the time dependence of the different subbands varies in the initial stages, and that only after about 5 h or so, all subband intensities

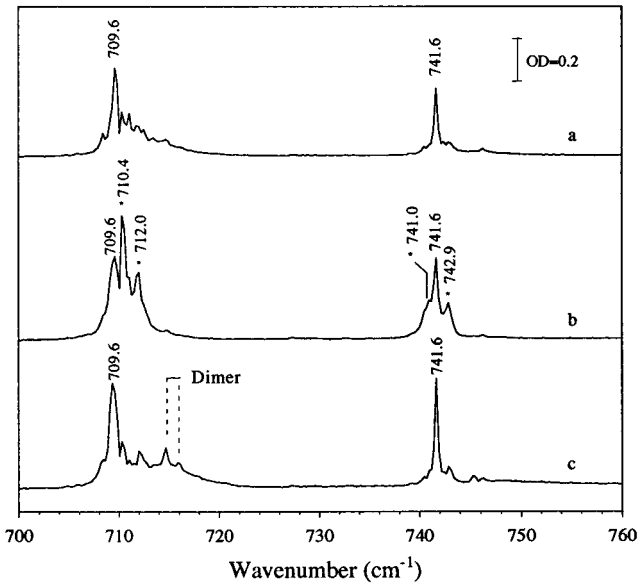

Figure 4. A portion of the IR spectrum of CHT in argon under different experimental conditions (bands marked by asterisks are assigned to metastable sites): (a) 1:3025 deposited at 23 K, spectrum taken at 13 K. (b) 1:1300 deposited at 14 K, spectrum taken at 14 K. (c) Same as (b) after annealing at 38 K for 20 min; spectrum taken at 14 K.

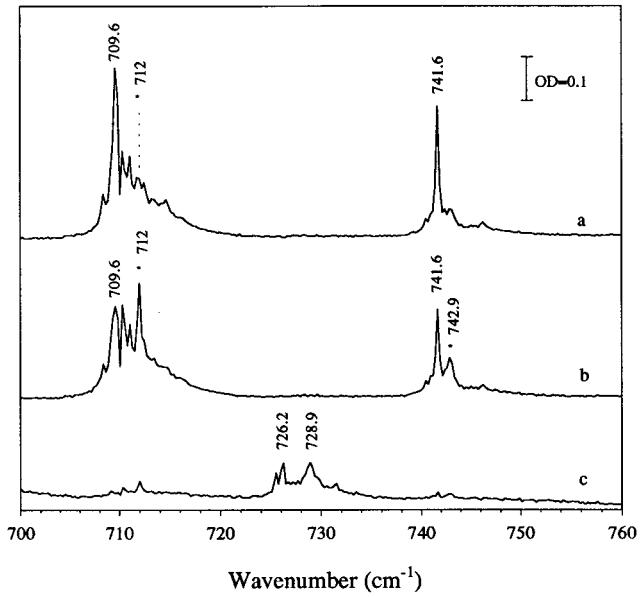

Figure 5. A portion of the IR spectrum of CHT in argon before and after irradiation at 2537 Å (bands marked by asterisks are assigned to metastable sites): (a) as in Figure 4a, (b) after 1 h of irradiation, (c) after 90 h of irradiation.

decreased at approximately the same rate. The intensity of the 711.9 subband is seen to *increase* initially by almost 20%, before it begins to decrease. In contrast, no difference in the formation rate of the different *product* subbands could be discerned—all appeared to grow at the same rate. Admittedly, the signal-to-noise ratio at the very beginning of the reaction did not allow detecting minor (<20%) differences.

3.1.3. Characterization of the Product. Prolonged irradiation results in almost complete conversion to the product. (90% in argon and >95% in N_2). The relative strength of the extinction coefficient of CHT and the product can be determined by analyzing an experiment in which a complete conversion of CHT to product was obtained. Assuming, on the basis of the IR spectra, that only one product is formed, the relative areas

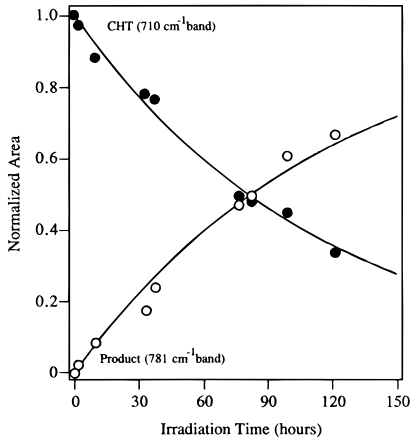

Figure 6. Reactant and product total IR band intensities as a function of irradiation time in an argon matrix. The data were fitted to a first-order decay of CHT and rise of the product (solid lines). An independent fit led to a unimolecular rate constant of $(8.4 \pm 0.3) \times 10^{-3}$ h^{-1} for CHT decay and $(8.6 \pm 0.3) \times 10^{-3}$ h^{-1} for the product's formation.

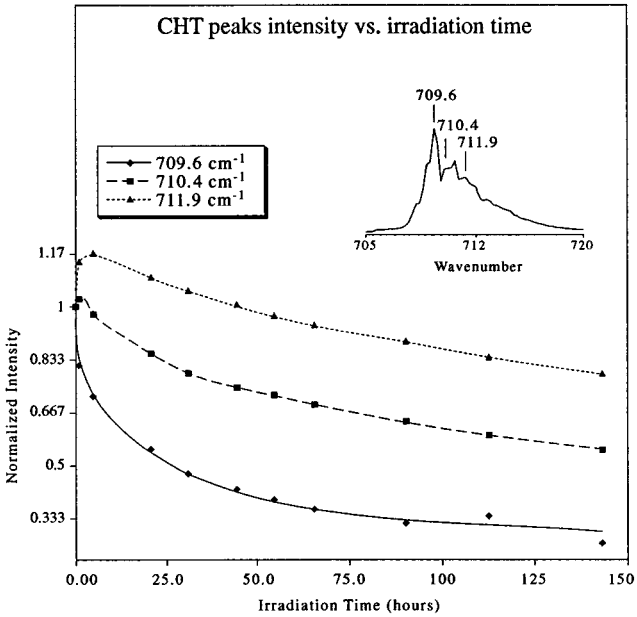

Figure 7. Individual subband intensities of the CHT 710 cm^{-1} band in an argon matrix as a function of irradiation time (the intensities of each subband are separately normalized the initial value). The inset shows the initial intensity distribution before irradiation was started.

of the two strongest peaks of both CHT and the product will be equal to the ratio of the extinction coefficients of the two bands. For CHT in argon the ratio of the area under the absorption bands of the two strongest bands (710 cm^{-1} in CHT to 782 cm^{-1} in BCHD) is found to be 2.5:1. A similar value was obtained for a nitrogen matrix (discussed in the next subsection): the ratio of the integrated area of the corresponding CHT and product bands in that matrix was found to be 2.2:1. The average ratio is thus 2.35.

The product IR absorption bands, as those of CHT, are found to be split. They typically consist of four main subbands, as for example, the 782 cm^{-1} product band exhibits four maxima at 780.8, 781.4, 782.1, and 783.4 cm^{-1}. Their relative intensities are found to be constant under different deposition and irradiation conditions. However annealing by rapid heating to 35 K and then recooling to 13 K leads to considerable changes in the relative intensities of the subbands, as shown in Figure 8. For instance, there is a dramatic decrease in the 780.8 and

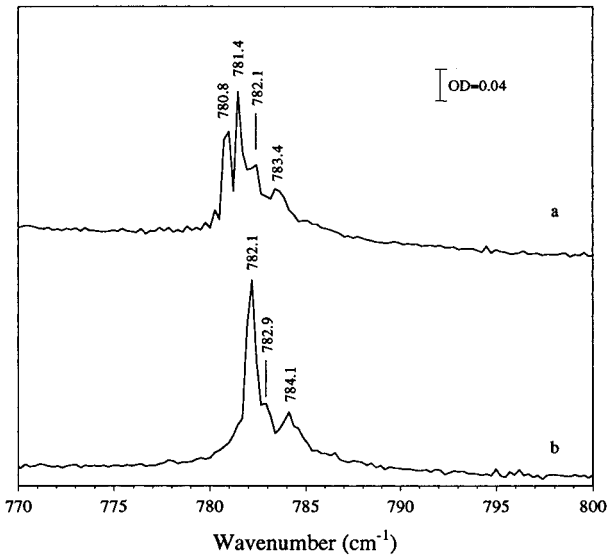

Figure 8. Annealing effect on the product's subband structure at 781 cm^{-1} in an argon matrix. Top: a 1:3000 matrix deposited at 23 K and irradiated at 13 K for 90 h at 23 K. Bottom: same matrix after annealing at 35 K for a few minutes, and recooling to 13 K.

TABLE 2: CHT Photochemical Depletion as a Function of Guest/Host Ratio in an Argon Matrix[a]

initial CHT:argon ratio	irradiation time (min)	conversion (%)
neat film	1338	2.1
1:100	1400	23
1:1280	1494	52
1:3000	1270	59

[a] All matrices deposited and irradiated at 23 K, except the 1:3000, which was irradiated at 13.5 K.

781.4 cm^{-1} peaks and a concomitant increase in the 782.1 peak.

3.1.4. Effect of CHT Concentration on Reaction Rate and Yield. The reaction's rate and yield were found to depend strongly on the initial reactant (CHT) concentration. Thus in a typical experiment, the total amount of CHT was about 3 times larger in a highly concentrated sample (Ar:CHT = 100) than in a more dilute one (Ar:CHT = 1300), as estimated from the optical density of the sample, yet after about 4 h of irradiation the product peak was found to be about 10 times more intense in the latter. Table 2 compares the reaction yield as a function of CHT concentration, for similar extended irradiation periods. It is obvious that both the rate and yield of the photochemical reaction of CHT are decreased as its concentration increases.

3.2. CHT in a N_2 Matrix. In general, the IR spectra and photochemical characteristics of CHT in a N_2 matrix were very similar to those observed in an argon matrix. The main IR bands of both CHT and the product were found to be split, indicating the coexistence of several trapping sites. UV irradiation led to a decrease in the CHT absorption bands; Initially the different subbands displayed different intensity changes, while upon prolonged irradiation, all bands decreased, leading eventually to complete disappearance of the CHT. The product's absorption bands were also split, but all subbands were found to grow at the same rate.

The two CHT IR bands discussed in section 3.1.1 were found to be slightly blue shifted (by ~3 cm^{-1}). Upon deposition at 23 K, each band is found to be split into two main subbands separated by 0.7 cm^{-1}: the 713 band into 713.7 (the dominant one under these conditions) and 713.0 cm^{-1}, and the 744 cm^{-1} band into 743.5 and 744.2 cm^{-1}. Deposition at 13 K led to a different relative intensity of the subbands, while annealing led to a major change: the stronger peak at 713.7 cm^{-1} almost disappeared, and the peak at 713.0 cm^{-1} became the dominant one by far. In addition, the intensity of three minor peaks at 717.5, 720.9, and 723.1 cm^{-1} was found to grow. These peaks become the most dominant ones when heating to 34 K, and are assigned to dimers or higher aggregates.

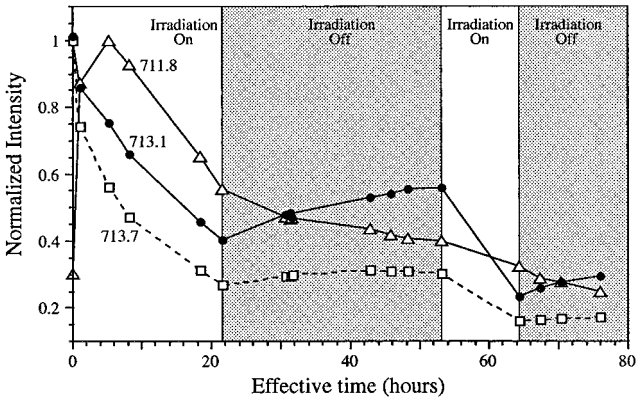

Figure 9. The time dependence of different IR subbands intensities of the CHT 713 cm^{-1} band during an extended irradiation experiment in a N_2 matrix containing CHT, showing both irradiation and dark periods (1:1400 matrix deposited at 23 K).

As in the argon matrix UV irradiation affected the subbands intensity selectively in the initial stages, with some showing an absolute intensity *increase*; further irradiation reduces all CHT subbands decrease, leading eventually to complete conversion to the product. Also in agreement with argon matrices, the relative intensities of the product subbands induced by the irradiation remained constant throughout.

Minor differences may be noted between the two matrices. Thus, in a N_2 matrix, relative and absolute intensity changes of CHT subbands caused by short-term irradiation were found to be reversed in the dark even at 23 K. Similar changes in an argon matrix required a higher temperature (>30 K). Figure 9 shows the intensity changes in the individual subbands of the 713 cm^{-1} feature as a function of time. It is seen that in the N_2 matrix the 713.1 cm^{-1} subband decreases strongly in the initial irradiation period and *increases* significantly during a dark period starting after 20 h of irradiation. A similar recovery effect, of a smaller magnitude, is found for the 713.7 cm^{-1} band that also undergoes immediate decrease upon irradiation. In contrast, the 711.8 cm^{-1} band, which increases initially upon irradiation, decreases during the dark period. It should be noted that, during the "dark" period, the *overall band intensities of both reactant and product did not change*, showing that no net chemical change occurred during that time.

As in the case of the corresponding argon matrix experiment, the kinetics of both reactant decay and product rise could be fit with first-order rate constants. The best fit rate constant for the CHT decay ($4.7 \times 10^{-2} \pm 4 \times 10^{-3}$ h^{-1}) is quite close to the independently obtained one for the product formation ($5.5 \times 10^{-2} \pm 3 \times 10^{-3}$ h^{-1}). These rate constants are significantly larger than the corresponding ones measured in an argon matrix.[47]

4. Data Analysis

4.1. Identification of the Product. The appearance rate of all new IR bands observed upon irradiation of CHT in either matrix was the same, indicating that only one stable product is formed. The product was identified from the IR spectrum as BCHD, based on comparison with published spectra[18] and on

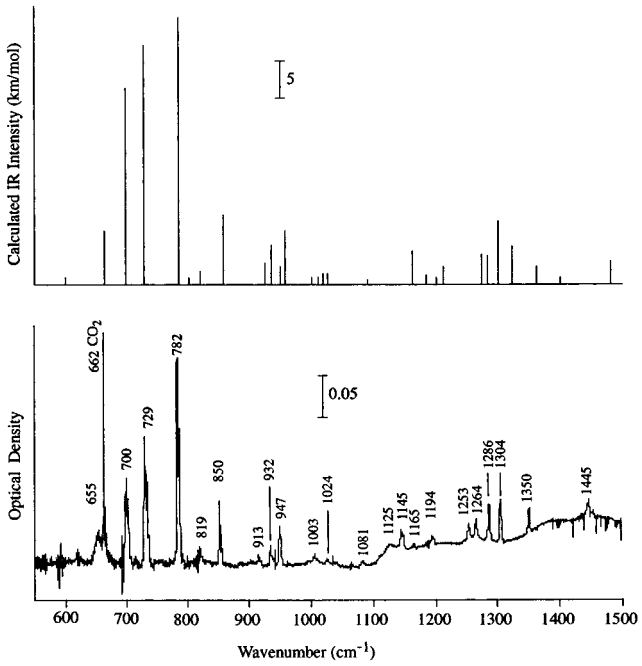

Figure 10. A portion of the IR spectrum of the product in a N_2 matrix compared to a quantum chemical density functional theory calculation of BCHD (B3LYP/6-311G* with a 0.988 correction applied).

quantum chemical calculations. Figure 10 shows the new IR bands induced by the UV irradiation, after almost complete conversion of CHT has been attained. No toluene bands were observed, in agreement with previous condensed phase studies. All CHT bands are very weak, almost unobservable. The figure shows also the ab initio calculated bar spectra of BCHD. Table 3 lists all the IR product bands and their relative intensities (normalized integrated area under the IR band) in the nitrogen matrix. The ab initio calculation was found to reproduce the experimental determination of the IR absorption intensity ratio of the CHT 710 cm^{-1} peak to that of the product's 782 cm^{-1} peak (section 3.1.3.). The experimental value is 2.35 ± 0.2, and the calculated one is 2.1. Thus, the accumulated evidence strongly indicates that BCHD is the main product under the present experimental conditions.

Table 4 compares the calculated and experimental data for CHT, and presents the BCHD calculations. The calculated structures were used for the MD simulations presented in section 5.

4.2. Trapping Sites Exchange. The subbands observed in the CHT spectra at high dilution (<1:1000) are assigned to different trapping sites. Other possible causes for the appearance of band splittings (different conformational isomers, hot bands or aggregates) may be ruled out. CHT has only one structural conformer, the temperature is too low for any hot bands to appear, and absorption peaks due to aggregation are observed only at higher concentration. Dimer (or possibly higher aggregates) peaks can be identified from their broad line shape and their assignment can be ascertained by heating to a high temperature in which the argon matrix starts to melt and dimers are formed. For example, for the 710 cm^{-1} band of CHT in argon, the dimer peak appears at 714.7 cm^{-1}, and for the 742 cm^{-1} band of CHT, it seems to be at 746.2 cm^{-1}. Initially these dimer peaks are weak and broad; they grow when annealed to high temperatures (see Figure 4c) and become the only peak in the respective CHT bands after heating to 44 K (not shown).

Annealing causes significant changes in the monomer peaks as well. It allows the qualitative determination of site stability,

TABLE 3: Experimental and Calculated Vibrational Frequencies of the Product BCHD

experimental			calculated	
frequency[a] (cm^{-1})	frequency[b] (cm^{-1})	normalized intensity	frequency[c] (cm^{-1})	intensity (km/mol)
185			188	0.0
256			260	1.2
401			406	1.6
471	475	3.1	474	4.8
663	655	2.6	662	7.6
697	700	60.8	696	27
728	729	82.1	727	33
782	782	100	784	36
820	819	6.7	819	2.0
832	850	21.8	855	9.7
882			885	0.1
911	913	2.7	921	3.0
934	932	9.9	931	5.4
946			946	2.4
1002	947	20.2	955	7.3
1008	1003	4.8	1008	1.0
1023	1024	2.9	1017	1.6
1077	1081	4.3	1025	1.5
1107	1125	9.3	1089	0.8
			1119	0.3
1141	1145	12.7	1160	4.7
1159	1165	3.3	1182	1.4
1190	1194	2.6	1209	2.6
1250	1253	8.7	1272	4.2
1260	1264	10.9	1282	4.0
1281	1286	21.2	1300	8.7
1299	1304	18	1323	5.2
1345	1350	12.3	1362	2.5
1439	1445	17.4	1481	3.1
1557			1612	1.9
1607			1655	1.1
2940	2850	20	2973	50
2911	2913	41	2992	29
	2920	32	2997	39
2939	2928	21	3028	66
3043	2943	43	3114	22
3050	2949	27	3118	17
	2955	22	3144	48
3116	3061	25	3148	31

[a] Reference 18. [b] Product IR spectra in a nitrogen matrix, this work. [c] B3LYP/6-311G* calculation, this work.

thus the 709.6 cm^{-1} subband (in an argon matrix) is due to the most stable site in the 710 cm^{-1} band region. UV irradiation also causes changes in the sites' relative populations, as determined from the IR spectrum. Moreover, some subbands are found to increase their absolute intensity, indicating net population transfer from other sites. In this case, other sites appear to be populated preferentially. These photochemically generated sites (such as the one leading to the 712.0 cm^{-1} subband) are not the thermodynamically most stable ones. The mechanism of their formation is discussed in section 6.2.

4.3. A Kinetic Model. The sole appearance of BCHD upon UV irradiation is in line with the model suggested by Srinivasan[2] that BCHD is formed on an excited state surface, contrary to toluene that is formed from a vibrationally hot ground state. The reaction is photochemically allowed according to the Woodward−Hoffmann rules—the ring closure of butadiene to cyclobutene. A likely scenario is the crossing to another singlet state (see section 1), which undergoes 1,7 H migration quite efficiently, and ring closure as a minor channel. Under the conditions of the present experiments, the hydrogen shift does not lead to a chemically distinct product, and the only net product is BCHD. Since the latter absorbs very weakly at 2537 Å, prolonged irradiation leads to almost complete conversion

TABLE 4: Calculated and Experimental Rotational Constants and Enthalpy for CHT and BCHD

	CHT experimental	CHT calculated[a]	BCHD calculated[a]
rotational constants (MHz)			
A	3696.11 ± 0.02[b]	3683.70	5036.50
B	3672.09 ± 0.02	3680.85	3140.58
C	2032.30 ± 0.01	2015.86	2317.23
enthalpy			
E (hartree)		−271.568 251 7	−271.531 528 7
ΔH^{zpe} (kcal/mol)[c]		80.11	79.76
ΔH^{react} (kcal/mol)[d]	22.69		
dipole moment (debye)			
x	0.24 ± 0.04	0.258	0.046
y	−	0.000	−0.119
z	0.060 ± 0.002	0.153	0.024

[a] All calculated values from B3LYP/6-311G* calculations, this work. [b] CHT experimental values from ref 10. [c] Zero point vibrational energy. [d] $\Delta H^{react} = \Delta H(\text{BCHD}) + \Delta H^{zpe}(\text{BCHD}) - \Delta H(\text{CHT}) - \Delta H^{zpe}(\text{CHT})$

of CHT to BCHD, as expected in a photostationary equilibrium. The lower yields previously observed at room temperature in condensed phases[7] may be explained by some hot band absorption of BCHD, leading to a smaller final BCHD/CHT concentration ratio in the photostationary state.

The initial *increase* in the absorption intensity of some IR subbands of CHT upon UV irradiation may be qualitatively explained by the following kinetic model, based on the assumption that the subbands are due to different trapping sites. For simplicity we assume that there are three spectroscopically distinguishable sites, denoted as A, B, and C. The concentration of CHT in these sites will be denoted as [A], [B], and [C], respectively. The product appears in several spectroscopically distinct sites, but since they are kinetically indistinguishable, we lump them together in the model, and denote the total concentration of the product by [P].

The rate constants to form P are assumed to differ significantly: for A it is highest, B is nonreactive, and C is assumed to be much less reactive than A. To reproduce the initial rapid decay of A, and rise of B, they are assumed to be in relatively rapid equilibrium. The simplest mechanism that was found to approximately reproduce the data required that only A, the more reactive site, will also be converted to the less reactive one, C, and that C, in turn, may be converted to B. This "bare bones" mechanism is represented by the following equations:

$$A \underset{K_{ba}}{\overset{K_{ab}}{\rightleftharpoons}} B$$

$$A \xrightarrow{K_{ap}} P$$

$$A \xrightarrow{K_{ac}} C$$

$$C \xrightarrow{K_{cp}} P$$

$$C \xrightarrow{K_{cb}} B$$

The concentrations appearing in the model are of the ground-state species; the reactions are all light induced, so that the rate constants include light intensity and the absorption coefficients, which were assumed to be equal for all sites. The absorption of the product at 2537 Å is negligible, so that no back reaction is included in the mechanism. The rate constants were fitted to reconstruct the experimental data of Figure 7 (CHT in argon). Initial concentrations were taken from the experimental values with the assignments: A, the species absorbing at 709.6 cm^{-1}; B, the species absorbing at 711.9 cm^{-1}; C, the species absorbing at 710.4 cm^{-1}. The concentration of the product is found from

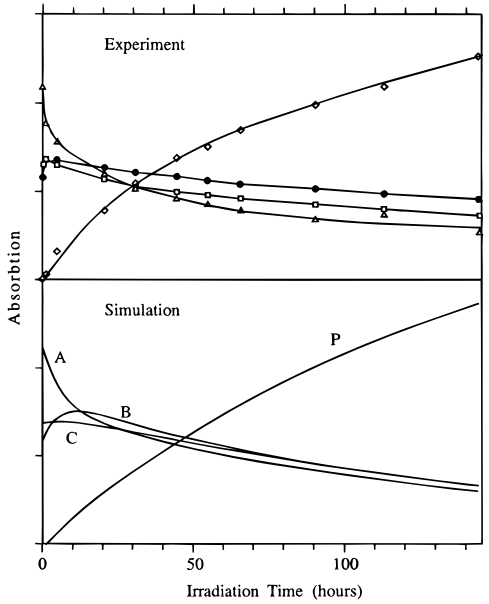

Figure 11. The time dependent population of different sites according to the kinetic model.

conservation of matter

$$[P(t)] = [\text{CHT}(0)] - \{[A(t)] + [B(t)] + [C(t)]\}$$

The best fit results are shown in Figure 11. The derived rate constants are as follows (units: h^{-1}): $k_{ab} = 7.2 \times 10^{-3}$; $k_{ba} = 9 \times 10^{-3}$; $k_{ac} = 1.6 \times 10^{-3}$; $k_{cb} = 1.8 \times 10^{-3}$; $k_{ap} = 1.8 \times 10^{-3}$; $k_{cp} = 2.7 \times 10^{-4}$. A more elaborate model is required for a quantitative reproduction of the experimental data, but even the simple one indicates that site interconversion with realistic rate constants accounts for the data.

5. MD Simulations

Molecular dynamics simulations of the argon matrix deposition and trapping site formation were carried out to provide an insight into the structure of the trapping sites in argon. In particular, we were interested in accounting for the reactivity differences of different sites. The basic procedure of the simulation was described in detail previously.[34−36] The interactions between the particles were assumed to be sums of atom−atom pairwise Lennard-Jones potentials, with the parameters listed in the references cited. All depositions were done on the fcc 100 crystal plane, the total number of argon atoms being about 800. In the present simulations the CHT and BCHD

molecules were treated as rigid bodies (using the RATTLE algorithm[39]), their structures being taken from the ab initio calculations.

It was found that the smallest trapping site of CHT was a four-substituted one, while that of BCHD was a five-substituted one. However, for both molecules larger sites were also obtained, with a relatively high probability. The most probable site sizes for both molecules were a five- or six-substitutional ones, the probability of larger ones falling off quite rapidly with size. The structure of some of these sites is shown in Figure 12. The attractive interaction between two argon atoms at the equilibrium separation is stronger than that between an argon atom and one of the first-row atoms constituting the molecules. Therefore it was found that the smaller trapping sites were in general energetically more stable than the larger ones.

The connection between the site structure as found from the MD simulations and IR spectral shifts was not established yet. It was found that some larger trapping sites were structurally similar to smaller ones. For instance, a four-substituted site could be formed by removing four argon atoms from a single 100 plane; a five-substitutional site was obtained by removing another argon atom either from the same crystallographic plane or from an adjacent one. In the latter case the IR shift of an in-plane vibration could be similar to that of the original four-substitutional site. It is therefore possible that each of the experimentally distinct subbands (observed with a 0.5 cm^{-1} resolution) represents several similar trapping sites.

An immediate result of the simulation is that some sites are expected to be less reactive than others. In particular, a four-substitutional site of CHT is too small to accommodate BCHD and cannot sustain a reaction. It may, however, be converted to a larger site, provided an argon atom adjacent to the molecule will diffuse away. We believe that the experimental results indicate that this must take place under irradiation (see section 6.2).

6. Discussion

6.1. Trapping Sites. The existence of several spectroscopically and kinetically distinct trapping sites of CHT in an argon matrix has been demonstrated. By using highly diluted mixtures (1:3000), we could rule out the possibility that any of these peaks is due to dimers or larger oligomers. Low-temperature deposition (14 K) leads to the same main IR subbands but with different relative intensities (i.e., populations) than those observed at higher deposition temperature. In general, deposition at higher temperatures (such as 23 K or 26 K for argon matrices) leads to a more ordered matrix (polycrystalline) in which less stable trapping sites are more rarely formed. Thus, subbands that are relatively more intense upon deposition at 14 K are likely to be due to unstable trapping sites. This assumption was substantiated by annealing experiments. Those peaks that are thought to arise from unstable trapping sites decreased in intensity, and the peak that is dominant when depositing at 23 K was the main feature left after annealing.

6.2. Mechanism of Irradiation Induced Site Exchange. UV irradiation changes the relative intensity of the different subbands within a specific CHT IR absorption band. In the initial stages of irradiation there is even an increase in the absolute intensity of one subband in both argon and N_2 matrices. Since different subbands were assigned to different trapping sites (or groups of sites), a plausible interpretation is population transfer from one site to another. The sites whose population increased are not the most stable ones, as deduced by comparison with the annealing experiments. Rather, they are the same ones that were relatively more intense when depositing at 14 K (i.e., metastable sites). A possible mechanism, proposed in the kinetic model, is conversion of some sites to less stable ones.

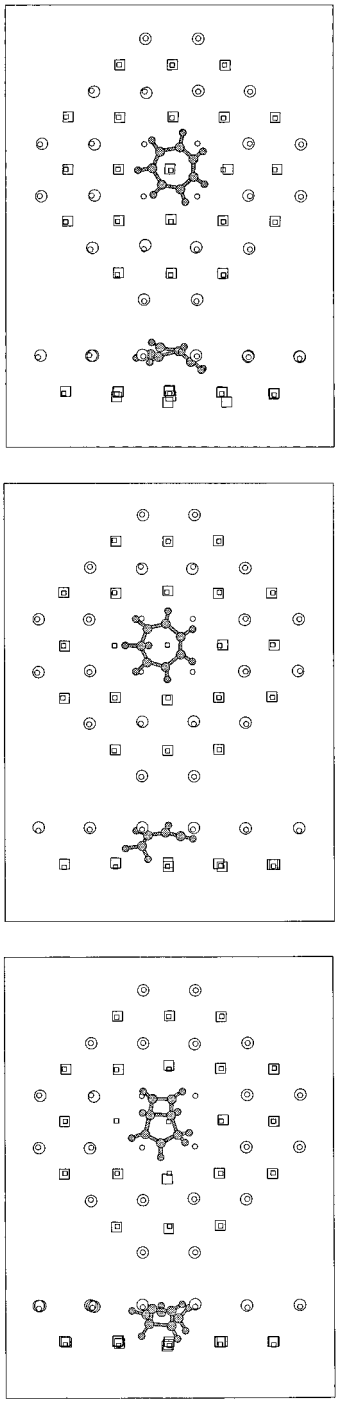

Figure 12. The structure of some MD calculated CHT and BCHD trapping sites in an argon matrix. The two lattice planes shown are those in which argon atoms were displaced by the trapped molecules. One of them is denoted by squares, the other by circles. The large symbols are the locations of argon atoms in the simulated matrix; the small ones are the locations of the argon atoms in a perfect fcc lattice. Deposition was on a 100 plane. (a) A four-substitutional site of CHT. (b) A six-substitutional site of CHT. (c) A six-substitutional site of BCHD (note the similarity to the six-substitutional site shown in (b).

The electronically excited molecules undergo rapid vibrational relaxation to the minimum of the excited state potential surface, followed by crossing to another surface, or planarization. Planarization is followed rapidly (on a 10^{-13} s time scale[40]) by H atom shift and reformation of CHT. This back and forth

skeletal "boat to boat" motion affects the surrounding argon atoms, allowing their reordering around the trapped molecule. A possible outcome is the formation of a non reactive four substituted site, from a five substitutional one.

The transformation of nonreactive sites to reactive ones under irradiation is also possible: the electronic energy is converted to vibrational energy in CHT, which can be exchanged with the surrounding matrix. A likely site exchange mechanism is the migration of an argon atom (or a N_2 molecule) from the immediate vicinity of the molecule to a vacancy somewhere else in the matrix. This restructuring requires, as a rule, the relocation of several matrix atoms, and therefore is a relatively rare event. In other words, molecules residing in a nonreactive site are recycled many times back and forth between the ground and the excited states before isomerization can take place in the reactive sites. As the population of the reactive sites decreases, the photostationary equilibrium depletes also the nonreactive ones.

The combined evidence of the MD simulations and the kinetic model can be used to speculate on the structure of the different sites: the more reactive site (A in the kinetic model) is likely to be a six-substitutional site in which either four matrix atoms were removed from one lattice plane and two from an adjacent one (a 4+2 6S site as shown in Figure 12b), or five matrix atoms from one lattice plane and one from the other (5+1 6S site). These two sites may actually be easily interchangeable under illumination. The less reactive site (C in the kinetic model) may be a 4+1 five-substitutional (5S) site, and the nonreactive one (B in the kinetic model) a 5+0 substitutional one. Site C can be formed from the more reactive A site by the migration of a single argon atom into a vacancy, and it can be transformed into the less reactive one by the migration of a vacancy from one lattice plane to a neighboring one.

An interesting distinction between the experiments in Ar and in N_2 is that in the dark period after irradiation at 23 K the relative intensities of different subbands are observed to change, while they remain constant in the argon matrix unless the matrix is warmed to a higher temperature (30 K). It was verified that CHT peaks in a N_2 matrix do not exhibit any change at 23 K if the matrix was not previously exposed to UV irradiation. The different "dark time" behavior is probably due to the larger reactivity of N_2 matrices:[24,41] the stress induced by the irradiation may be partially relieved in a nitrogen matrix by rearrangement of the matrix molecules involving, for instance, rotational motion. This motion is typically characterized by low energetic barriers, allowing the thermal motion to surmount it even at 23 K. A similar effect was noted by Raducu et al. for conformer interconversion.[42]

6.3. Reaction Mechanism. Our discussion of the reaction mechanism is based on the twin state concept for isomerization reactions. As shown elsewhere,[43] the wave function representing the transition state of valence isomerization reactions (in distinction from conformational isomerization) may be constructed in a valence bond representation from combinations of the reactant and product wave functions. Two combinations are possible, an in-phase and an out-of-phase one, which are referred to in the following as the conjugate, or twin states, to denote their common parentage. If the transition state has an "aromatic" character, the combination representing it is an in-phase one and transforms as the totally symmetric representation of the symmetry group to which the transition state belongs. The out-of-phase one represents an excited state and transforms as one of the nontotally symmetric representations. If the transition state is "anti-aromatic", it is an out-of-phase combination and transforms as a nontotally symmetric representation, while the conjugate excited state is constructed from the in-phase combination and transforms as the totally symmetric representation. The aromatic transition state is defined as one in which an odd number of electron pairs participates in a pericyclic reaction, while in an antiaromatic one, the number of participating electron pairs is even. It has been shown that the two conjugate states are similar in structure, the minimum of the excited state being located at the same position along the reaction coordinate as the transition state. Furthermore, it was shown that the gap between the two states is large for an "aromatic" transition state and small for "anti-aromatic" ones. Typical values are 5 and 2 eV, respectively.

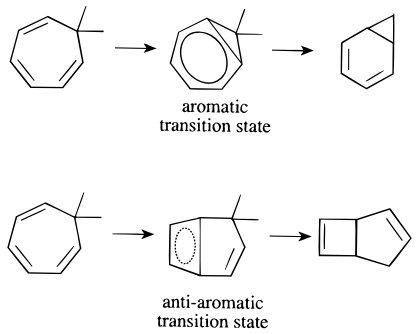

Figure 13. A scheme showing the assumed transition states of two CHT isomerization reactions: an aromatic one to norcaradiene and an anti-aromatic one to BCHD.

In the cycloheptatriene system, the transition state to form norcaradiene (leading to toluene) is aromatic, while the transition state to form BCHD is antiaromatic (Figure 13). Therefore, the conjugate excited state of the former is above the initially excited state of CHT, while that of the latter is lower.

UV absorption at 2537 Å is known to populate the $1^1A''$ state, which is depopulated by ultrafast processes (within ~60 fs) as found by multiphoton ionization studies.[40] The most plausible explanation is coupling to another electronically excited state of A′ symmetry, whose existence is supported by magnetic circular dichroism[46] and resonance Raman experiments.[15,17] The scheme, shown in Figure 14, is compatible with previous data and accounts for the present experiments. The vibrationally excited $1^1A''$ state formed initially by the light absorption can lead to toluene production by rapid internal conversion to the ground state. The conjugate excited state of the "aromatic" transition state between CHT and norcaradiene, Q in the figure, is too high lying to be involved. In the gas phase this is indeed the dominant process, leading to toluene as the major product. Toluene is formed via norcaradiene followed by a biradical intermediate. In the condensed phase, this route is practically blocked by rapid vibrational relaxation, allowing other processes to take place.

The lower vibrational states of the $1^1A''$ state are coupled to another electronically excited state (the most likely candidate being $2^1A'$). It appears to have several minima along different coordinates; one, (Z in the Figure), which is the conjugate of the transition state between CHT and BCHD; another, Y in the figure, is thought to lead to the 1,7 hydrogen shift.[8,15,17] Z is a low-lying excited state, being conjugate to an antiaromatic transition state. It is coupled via a conical intersection to the ground-state surface, at the transition state. The system may then revert to the reactant CHT, or proceed to form the product. The former is the statistically preferred process, since the CHT minimum is much lower than the BCHD one,[44] but since it leads to no net reaction, is unobservable. Since BCHD does not

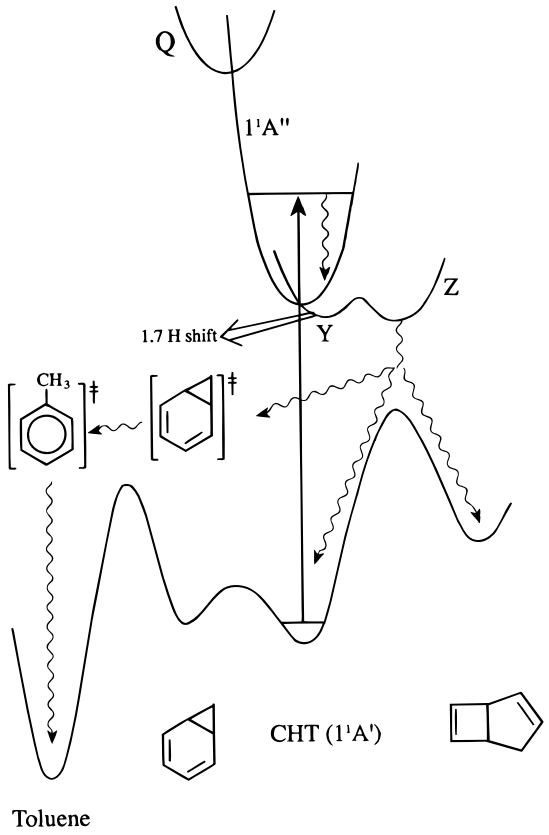

Figure 14. A schematic representation of CHT photochemical transformations. The energies of the known compounds are taken from Figure 2. Z, the conjugate of the transition state between CHT and BCHD, and Y denote two local minima along different coordinates, both probably lying on the $2^1A'$ surface referred to in ref 17. The transition from the S_1 ($1^1A''$) CHT state to norcaradiene probably takes place on the ground state potential surface. Formation of toluene from norcaradiene may involve a biradical intermediate (not shown). The 1,7 H shift reaction takes place along a different reaction coordinate than the other two reactions, leading eventually to CHT ground state. The wavy lines denote vibrational relaxation.

absorb at 2537 Å, the system's photostationary equilibrium eventually favors it in a cryogenic matrix, even though the rates of competing deactivation processes are faster than the route leading to it.

In the present experiments spectroscopically distinct trapping sites were found to exhibit different kinetic behavior; this was clearly observed in the initial stages of the photolysis. Nonetheless, the product site distribution, as revealed in the IR band splitting, is the same regardless of the initial site nature. In addition, the product's appearance rate in all sites is the same. Annealing is found to change drastically the relative intensities of the subbands showing that the photochemically generated sites are not the energetically most stable ones. The most likely mechanism accounting for these observations is the following: since the majority of the excited molecules are recycled to the CHT ground state, site restructuring is the major process taking place, by the mechanisms discussed in Section 6.1. Reaction to form BCHD is due mostly to a given site or group of sites, leading to the observed product site distribution. The formation of BCHD from a suitable site is done by a sequence of curve crossings and conical intersections, so that along the way the system is never highly vibrationally excited and "slides" along the electronic surface. Therefore, the local environment is never strongly heated locally, explaining the absence of self-annealing.

A further finding is the strong self-quenching of the reaction observed upon increasing CHT concentration (section 3.1.4). A similar effect was found also in liquid solution experiments. This self-quenching is suggested to be due to coupling between ground-state neighboring CHT molecules and one of the electronically excited states involved in the process, possibly by the formation of an exciplex state. These results and the fact that different sites reacted with different rates we deduce that a reaction occurs mostly in an isolated site and not in molecular aggregates.

Summary

The UV photolysis of cycloheptatriene (CHT) in cryogenic matrices leads essentially exclusively to the formation of bicyclo[3.2.0]hepta-2,6-diene (BCHD). A clear kinetic site effect is found: different trapping sites exhibit different reaction rates. This effect is accounted for by a molecular dynamic simulation of trapping site structure, showing that some sites are more likely to react than others. The eventual quantitative conversion of CHT to BCHD is consistent with a kinetic model that includes light induced site interconversion steps. The model qualitatively accounts also for the individual sites' population changes. An energy level diagram of this C_7H_8 system provides a qualitative account for the predominance of BCHD product in condensed phases and of toluene in the gas phase.

Acknowledgment. This work was supported by the Israel Science Foundation. We are indebted to Dr. S. Zilberg for many enlightening discussions. The Farkas Center for Light Induced Processes is supported by Minerva mbH, Munich. We thank one of the referees for an enlightening discussion of the proposed mechanism.

References and Notes

(1) Dauben, W. G.; Cargill, R. L. *Tetrahedron* **1961**, *12*, 186.
(2) Srinivasan, R. *J. Am. Chem. Soc.* **1962**, *84*, 3432.
(3) Thrush, B. A.; Zwolenik, J. J. *Bull. Soc. Chim. Belg.* **1962**, *71*, 642.
(4) Ter Borg, A. P.; Kloosterziel, H. *Recueil* **1965**, 84, 241; *Recueil* **1969**, *88*, 266.
(5) Luu, S. H.; Troe, J. *Ber. Bunsen-Ges. Phys. Chem.* **1973**, *77*, 325.
(6) Paulick, W.; Abraham, W.; Jung, C.; Kreysig, D. *Mol. Photochem.* **1979**, *9*, 443.
(7) Daino, Y.; Hagiwara, S.; Hakushi, T.; Inoue, Y.; Tai, A. *J. Chem. Soc., Perkin Trans. II* **1989**, 275.
(8) Reid, P. J.; Wickham, S. D.; Mathies, R. A. *J. Phys. Chem.* **1992**, *96*, 5720.
(9) Traetteberg, M. *J. Am. Chem. Soc.* **1964**, *86*, 4265.
(10) Butcher, S. S. *J. Chem. Phys.* **1965**, *42*, 1833.
(11) Anet, F. A. *J. Am. Chem. Soc.* **1964**, *86*, 458.
(12) Jensen, F. R.; Smith, L. A. *J. Am. Chem. Soc.* **1964**, *86*, 956.
(13) Saebo, S.; Boggs, J. E. *J. Mol. Struct.* **1982**, *87*, 365.
(14) Cremer, D.; Dick, B.; Christeu, O. *J. Mol. Struct. (THEOCHEM)* **1984**, *110*, 277.
(15) Reid, P. J.; Shreve, A. P.; Mathies, R. A. *J. Phys. Chem.* **1993**, *97*, 12691.
(16) Zuccarelo, F.; Buemi, G.; Raudino, A. *J. Comput. Chem.* **1980**, 1, 341.
(17) Reid, P. J.; Lawless, M. K.; Wickham, S. D.; Mathies, R. A. *J. Phys. Chem.* **1994**, *98*, 5597.
(18) Evans, M. V.; Lord, R. C. *J. Am. Chem. Soc.* **1961**, *83*, 3409.
(19) Willcott, R. M.; Goerland, E. *Tetrahedron Lett.* **1966**, 51, 6341.
(20) Hippler, H.; Luther, K.; Troe, J.; Walsh, R. *J. Chem. Phys.* **1978**, 68, 323.
(21) Chung, G. Y.; Carr, R. W. *J. Phys. Chem.* **1987**, *91*, 2831.
(22) Klump, K. N.; Chesick, J. P. *J. Am. Chem. Soc.* **1963**, *85*, 130.
(23) Warner, P. M.; Lu, S. *J. Am. Chem. Soc.* **1980**, *102*, 331.
(24) Haas, Y.; Samuni, U. In *Reactions in Rare Gas Matrices—Matrix and Site Effects in Chemical Kinetics*; Compton, R., Hancock, G., Eds.; Blackwell Science Ltd.: Oxford, 1998. In press.
(25) Fraenkel, R.; Haas, Y. *Chem. Phys. Lett.* **1993**, 214, 234.
(26) Samuni, U.; Kahana, S.; Fraenkel, R.; Haas, Y.; Danovich, D.; Shaik, S. *Chem. Phys. Lett.* **1994,** *225*, 391.
(27) Jacobs, J.; Kronberg, M.; Muller, H. S. P.; Willner, H. *J. Am. Chem. Soc.* **1994**, *116*, 1106.

(28) Johnsson, K.; Engdahl, A.; Kolm, J. *J. Phys. Chem.* **1995,** *99*, 3902.
(29) Raff, L. M. *J. Chem. Phys.* **1990**, *93*, 3160; *J. Chem. Phys.* **1991**, *95*, 8901, 8905; *J. Chem. Phys.* **1992**, *97*, 7459.
(30) Alimi, R.; Gerber, R. B.; Apkarian, V. A. *J. Chem. Phys.* **1990**, *92*, 3551.
(31) Samuni, U.; Haas, Y. *Spectrochim. Acta A* **1996**, *52*, 1479.
(32) Benderskii, A. V.; Wight, C. A. *J. Phys. Chem.* **1996**, *100*, 1.
(33) Zuhse, R. H.; Wong, M. W.; Wentrup, C. *J. Phys. Chem.* **1996**, *100*, 3197. Kappe, C. O.; Wong M. W.; Wentrup, C. *J. Org. Chem.* **1995**, *60*, 1686.
(34) Fraenkel, R.; Haas, Y. *Chem. Phys.* **1994**, 186, 185.
(35) Fraenkel, R.; Kahana, S.; Haas, Y. *Ber. Bunsen-Ges. Phys. Chem.* **1995**, *99*, 412.
(36) Molnar, F.; Dick, B.; Fraenkel, R.; Haas, Y. To be published.
(37) Frisch, M. J.; Trucks, G. W.; Schlegel, H. B.; W. Gill, P. M.; Johnson, B. G.; Robb, M. A.; Cheeseman, J. R.; Keith, T.; Petersson, G. A.; Montgomery, J. A.; Raghavachari, K.; Al-Laham, M. A.; Zakrzewski, V. G.; Ortiz, J. V.; Foresman, J. B.; Cioslowski, J.; Stefanov, B. B.; Nanayakkara, A.; Challacombe, M.; Peng, C. Y.; Ayala, P. Y.; Chen, W.; Wong, M. W.; Andres, J. L.; Replogle, E. S.; Gomperts, R.; Martin, R. L.; Fox, D. J.; Binkley, J. S.; Defrees, D. J.; Baker, J.; Stewart, J. P.; Head-Gordon, M.; Gonzalez, C.; Pople, J. A. *Gaussian 94*, Revision D.4; Gaussian, Inc.: Pittsburgh, PA, 1995.
(38) Hehre, W. J.; Ditchfield, R.; Pople, J. A. *J. Chem. Phys.* **1972**, 56, 2257.
(39) Allen, M. P.; Tildesley, D. J. *Computer Simulations of Liquids*; Clarendon Press: Oxford, 1987.
(40) Borell, P. M.; Lohmannsroben, H.; Luther, K. *Chem. Phys. Lett.* **1987**, 136, 371; Fuss, W.; Hering, P.; Kompa, K. L.; Lochbrunner, S.; Schikarski, T.; Schmid, WQ. E.; Trushin, S. A. *Ber. Bunsen-Ges. Phys. Chem.* **1997**, *101*, 500.
(41) Schriever, A.; Schriever, L.; Perchard, J. P. *J. Mol. Spectrosc.* **1988**, *127*, 125.
(42) Raducu, V.; Jasmin, D.; Dahoo, R.; Brosset, P.; Gauthier-Roy, B.; Abouaf-Marguin, L. *J. Chem. Phys.* **1995** 102, 9235.
(43) Zilberg, S.; Haas, Y. Shaik, S. *Angew. Chem., Int. Ed. Engl.* **1998**. In press. An early discussion of the twin state concept applied to benzene is found in: Feynmann, R. P.; Leighton, R. B.; Sands, M. *Feynmann Lectures in Physics;* Addison-Wesley: New York, 1965; Vol. III, Chapter 10.
(44) Ben-Shaul, A.; Haas, Y. *J. Chem. Phys.* **1980**, 73, 5107.
(45) Lau, C. L.; Ruyter, H. D. *Spectrochim. Acta* **1963**, 19, 1559.
(46) Dauben, W. G.; Seeman, J. I.; Wendschu, P. H.; Barth, G.; Bunnenberg, E.; Djerassi, C. *J. Org. Chem.* **1972**, *57*, 1209.
(47) More detailed data concerning CHT nitrogen matrices (IR spectra, kinetics) are available from the authors upon request.